2020 IEEE/RSJ International Conference on Intelligent Robots and Systems (IROS)
October 25-29, 2020, Las Vegas, NV, USA (Virtual)

Simultaneous Estimation of Vehicle Position and Data Delays using Gaussian Process based Moving Horizon Estimation

Daiki Mori and Yoshikazu Hattori

***Abstract*— Automobiles or robots with advanced autonomous systems are equipped with multiple types of sensors to overcome different weather and geographical conditions. These sensors generally have various data delays and sampling rates. Additionally, the communication delays or time synchronization errors between the onboard computers significantly affect the robustness and accuracy of localization for autonomous vehicles. In this paper, the simultaneous estimation of vehicle position and sensor delays using a Gaussian process based moving horizon estimation (GP-MHE) is presented. The GP-MHE can estimate the unknown delays of multiple sensors with the resolution less than that of GP-MHE sampling rate. The localization performance of GP-MHE was confirmed using full-vehicle simulator, then evaluated in a real vehicle experiment on a highway scenario. Experimental result verified the sufficient localization accuracy of sub 0.3m using data that had irregular sampling rate and delay of more than 150ms. The proposed algorithm extends the capability of integrating various data with large unknown delays for vehicles, robots, drones and remote autonomy.**

I. INTRODUCTION

Automobile or robots with advanced safety and autonomous systems require multiple types of sensors to overcome various weather and geographical conditions [1]. Sensors, such as the inertial measurement unit (IMU), camera, light detection and ranging (LiDAR), global navigation satellite system (GNSS) or vehicle to X (V2X) communication, have different sampling rates and time delays according to the complexity of the algorithm to retrieve vehicle information from raw data. Additionally, communication delays and time synchronization errors between the onboard computers significantly affect the robustness and accuracy of vehicle localization. Therefore, data time management in the advanced autonomous systems is one of the most fundamental challenge when fusing multiple sensor data.

In practice, the sensor fusion algorithms deal with sampling rates and delays ranging from 1 Hz to 200 Hz and 1μs to 400ms respectively. Furthermore, time synchronization errors and communication delays between the onboard computers are unknown in most cases. For example, a delay of 100ms at a speed of 100km/h is equivalent to a localization error of 27.7m/s$\times$0.1s=2.8m. Therefore, delay estimation is necessary to achieve sub-meter accuracy for vehicle localization.

The most typical sensor-fusion method for vehicle localization is Kalman filter. Extended Kalman filter (EKF), unscented Kalman filter (UKF) and particle filter(PF) are the modified versions of Kalman filter which has been applied to estimate the dynamic states of vehicles [2][3][4]. These filters are based on the first-order Markov chain, i.e, states X_N at time t_N is conditioned only on the previous state X_{N-1} at time t_{N-1} as shown in Fig. 1. Therefore, Kalman filters are useful for real-time implementation because data older than t_{N-1} do not need to be considered. However, Kalman filters have a significant limitation that data older than t_{N-1} cannot be used directly [5][6]. The Camera-IMU system was proposed to estimate camera delay [7]. However, the algorithm causes cumulative position error when propagating the states using IMU observation in the presence of long delay.

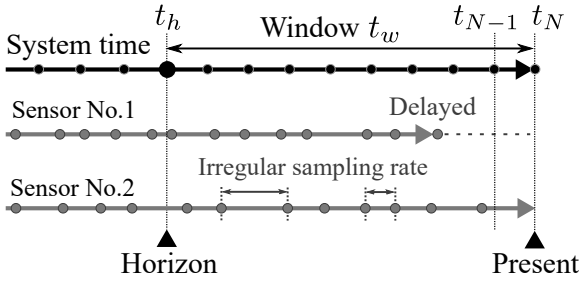

Fig. 1. System time and data time in a real vehicle system.

Moving horizon estimation (MHE) is the method that estimates the vehicle states within the time window as shown in Fig. 1 [8][9]. The key advantage of MHE against Kalman filters is that it can handle irregular sampling rates and delayed data without any additional modification [10]. Moreover, MHE utilizes all data acquired in the time window $t_h \sim t_N$; thus, it improves the estimation accuracy. The recent advancement in the model predictive control (MPC) can be applied to MHE for real-time implementation [11][12]. In addition, utilizing sparse matrix calculations can drastically improve computational speed [18]. MHE was also implemented to vehicle state estimation and its performance was equivalent to that of particle filter when there was no delays [13]. However, unknown time delays continue to be a fundamental challenge in MHE formulation.

As can be seen in Fig. 1, data delay causes data loss and irregular sampling rate causes miss alignment to the system time. To estimate the time delays with high accuracy, interpolation and extrapolation of data is necessary to match the system time. Gaussian process (GP) is an algorithm that can evaluate the interpolated and extrapolated data by standard deviation [14]. Additionally, GP is time differentiable so that it can be applied to MHE formulation.

In this paper, the simultaneous estimation of vehicle position and data delays using a Gaussian process based MHE

The authors are with Toyota Central R&D Labs. Inc., Nagakute, Japan
d-mori@mosk.tytlabs.co.jp

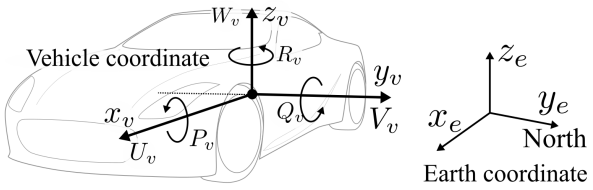

Fig. 2. Definition of vehicle coordinate system and earth coordinate system.

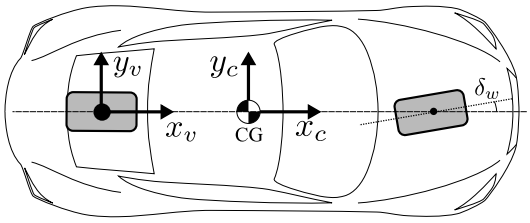

Fig. 3. Bicycle model.

(GP-MHE) is presented. The contribution of the proposed estimation method is as follows.

- Discrete observation data are converted to time differentiable functions by GP for nonlinear optimization.
- GP-MHE method is formulated that can simultaneously estimate vehicle states and unknown data delay times.

The GP-MHE extends the estimation target from the dynamic states to the time states. Therefore, the proposed method can simultaneously optimize both dynamics and time, thereby leading to accurate localization.

The rest of this paper is organized as follows. The state space model is formulated in Section II. The time delay and state estimation method using GP-MHE is presented in Section III. The proposed GP-MHE is validated using a full-vehicle simulator and experiment on a highway scenario in Section IV. Finally, the conclusion and future works are discussed in Section V.

II. VEHICLE DYNAMICS FORMULATION

The state space model for MHE is formulated in this section. The non-linear discrete state-space model is given in the following form.

$$x(k+1) = f(x(k),u(k)) + Q_n \quad (1)$$
$$y(k) = h(x(k),u(k)) + R_n \quad (2)$$

where f is the state propagation function, h is the observation function, x is the state, y is the observation, Q_n is the process noise, R_n is the measurement noise, k is the time-step and u is the input.

Coordinate systems are defined as shown in Fig. 2. The earth coordinate system is fixed to the earth surface with its y_e axis directed toward north. The x_v-y_v plane of the vehicle coordinate system is parallel to the road. The Euler attitude, velocity, angular velocity and moment of inertia of the vehicle are defined as $(\phi_v, \theta_v, \psi_v)$, $v_v = (U_v, V_v, W_v)$, $\omega_v = (P_v, Q_v, R_v)$ and (I_{xx}, I_{yy}, I_{zz}), respectively.

A. State space model

The vertical velocity and its differential value can be ignored ($W \approx 0, \dot{W} \approx 0$) since vehicle motions are restricted on the road surface. The same applies to the term $(I_{yy} - I_{xx})PQ$ for the rotational equation of motion. The errors due to the approximation of these can be included in the process noise. Thus, the equations of motion are obtained as follows.

$$\begin{cases} m(\dot{U}_v - R_v V_v) = F_x + mg\sin\theta_v \\ m(\dot{V}_v + R_v U_v) = F_y - mg\sin\phi_v\cos\theta_v \\ I_{zz}\dot{R}_v = N_v \end{cases} \quad (3)$$

where N_v is moment of force and force is $F = (F_x, F_y, F_z)$. The vehicle velocity for the vehicle coordinate system v_v can be converted to velocity on the earth coordinate system v_e by the rotation matrix R_x, R_y, R_y.

$$v_e = R_z^{-1} R_y^{-1} R_x^{-1} v_v \quad (4)$$

Further, the differentiation of the Euler attitude is given by the following equation.

$$\begin{bmatrix} \dot{\phi}_v \\ \dot{\theta}_v \\ \dot{\psi}_v \end{bmatrix} = \begin{bmatrix} 1 & \sin\phi_v\tan\theta_v & \cos\phi_v\tan\theta_v \\ 0 & \cos\phi_v & -\sin\phi_v \\ 0 & \sin\phi_v/\cos\theta_v & \cos\phi_v/\cos\theta_v \end{bmatrix} \omega_v \quad (5)$$

Yaw and lateral dynamics are formulated in the next section.

B. Vehicle model

A bicycle model with its origin at the center of the rear axle, shown in Fig. 3, is formulated. Organizing sensor information at the geometrically fixed rear axle is better than that at the center of gravity (CG), which changes. The lateral tire force at the front wheel F_f and rear wheel F_r is formulated as follows [15].

$$F_f = 2K_f\left(\delta_w - \frac{V_c + l_f R_v}{U_c}\right) \quad (6)$$
$$F_r = 2K_r\left(-\frac{V_c - l_r R_v}{U_c}\right) \quad (7)$$

where the velocity at CG is $v_c = (U_c, V_c, W_c)$, steer angle is δ_w, distance from the CG to the front and rear axles are l_f and l_r respectively, and the cornering stiffnesses of the front and rear wheels are K_f and K_r, respectively. The relation between the vector from the origin of the earth coordinate to the CG (r_{ec}), the vector from the origin of earth coordinate to the rear axle (r_{ev}), and the vector from the CG to rear axle (r_{cv}) are shown below.

$$\frac{dr_{ev}}{dt} = \frac{dr_{ec}}{dt} + \omega_v \times r_{cv} \qquad \left(\frac{\delta r_{cv}}{\delta t} = 0\right) \quad (8)$$

Therefore, by substituting $U_v = U_c$ and $V_v = V_c - l_r R_v$ to (3), (6), and (7), the bicycle model is formulated.

$$\frac{dR_v}{dt} = -\frac{2l_fK_f - 2l_rK_r}{I_{zz}U_v}V_v - \frac{2l_fK_fl}{I_{zz}U_v}R_v + \frac{2l_fK_f}{I_{zz}}\delta_w \quad (9)$$

$$\frac{dV_v}{dt} = -\frac{2K_f + 2K_r}{mU_v}V_v + \left(-U_v - \frac{2K_fl}{mU_v}\right)R_v + \frac{2K_f}{m}\delta_w - g\sin\phi_r\cos\theta_r - l_r\dot{R}_v \quad (10)$$

The state vector x is defined as follows.

$$x = [\, x_e\ y_e\ U_v\ \dot{U}_v\ V_v\ \phi_v\ \theta_v\ \psi_v\ P_v\ Q_v\ R_v\ \delta_w]^T \quad (11)$$

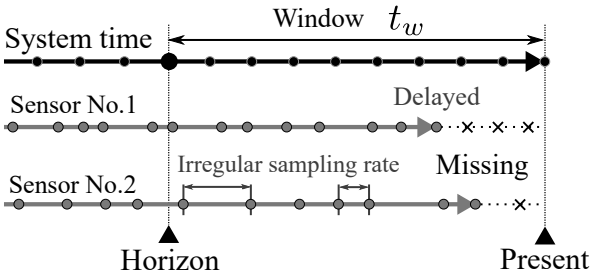

Fig. 4. Data loss due to time delays of sensors.

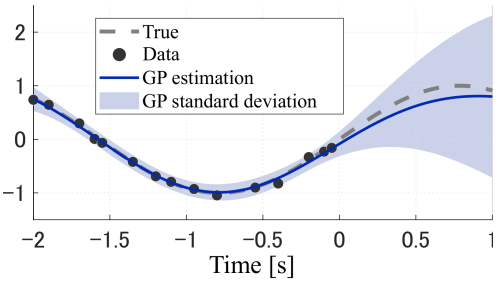

Fig. 5. An example of resampling and prediction with Gaussian process using data that has irregular sampling rate.

The state propagation equation (1) is formulated by the discrete form of (4), (5), (9), and (10). $\dot{U}_v, P_v, Q_v$ and δ_w are formulated as a random walk model. Hysteresis and compliance of the steering system, which is difficult to accurately model, can be included in the process noise by considering δ_w as one of the states. In this case, input u is zero vector.

III. Gaussian Process based Moving Horizon Estimation

MHE uses all the acquired data within the window time t_w and applies a nonlinear optimization algorithm to estimate the dynamical states. Here, the states are extended to time dimension to optimize both the dynamical states and the time states. MHE does not require any modification if the delay time is measured in advance [10]. In this study, time delays are considered as unknown values and MHE is modified using GP to optimize the vehicle states and data delays.

When the time delays are considered as unknown variable, the instance of missing data within the time window change according to the corresponding time delays, as evident in Fig. 4. Subsequently, the size of the cost function also changes. Therefore, discrete data must be resampled and predicted (interpolated and extrapolated) to fix the size of the cost function, and to align the data with system time. The resampling and prediction method should satisfy the following points.

- The method is capable of both interpolation and extrapolation.
- Resampling function is time differentiable for nonlinear optimization.
- The method is capable of calculating the accuracy (standard deviation) of the resampled or predicted data.

In this study, a GP is used so that the accuracy of the resampled and predicted data can be calculated via standard deviation [14], and satisfies all the conditions. First, GP is discussed and then, the GP-MHE is formulated in the following sections.

A. Gaussian process

Given the data $y_i \ \ (i = 1,2,...,n_d)$ acquired at time t_i $(i = 1,2,...,n_d)$, the aim is to resample and predict the data at time $t_i' \ \ (i = 1,2,...,n_h)$. the GP uses a function called kernel to define the correlation between data for interpolation and extrapolation [14]. With the GP, kernel is defined by a Gaussian distribution as below.

$$k(\alpha_i, \beta_j) \quad = \quad a_1 \exp(-\frac{|\alpha_i - \beta_j|^2}{a_2}) \tag{12}$$

where、a_1 and a_2 are Gaussian distribution parameters and α_i and β_i are time variables. Kernel matrix is defined as follows.

$$K_{ij}(\alpha, \beta) = k(\alpha_i, \beta_j) \tag{13}$$

Subsequently, the data $\hat{y}$ at time t' is derived.

$$\hat{y}(t') = f_{av}(t') = K(t,t')^T (K(t,t) + \sigma^2 I)^{-1} (y - \bar{y}) + \bar{y} \tag{14}$$

Where $\bar{y}$ is the mean of y and σ is the standard deviation of data. The variance can be calculated by the following equation.

$$\begin{aligned} Var(\hat{y}) =& f_{var}(t') \\ =& K(t',t') - K(t,t')^T (K(t,t) + \sigma^2 I)^{-1} K(t,t') \end{aligned} \tag{15}$$

It is important to note that both $f_{av}(t')$ and $f_{var}(t')$ are differentiable by time t' since kernel function is differentiable.

$$\frac{\partial k(\alpha_i, \beta_j)}{\partial \beta_i} = \frac{2a_1(\alpha_i - \beta_j)}{a_2} \exp(-\frac{|\alpha_i - \beta_j|^2}{a_2}) \tag{16}$$

Therefore, the Jacobian of the GP function can be derived for nonlinear optimization to estimate time delays. An example of GP with sine curve data is shown in Fig. 5. Future data are predicted with the standard deviation.

B. Conventional Moving Horizon Estimation

This section describes the conventional MHE without time delay estimation. Online MHE updates the state $X = [x_1, x_2, ..., x_{n_h}]^T$ once every time step using the nonlinear least-square Gauss-Newton method or the Levenberg-Marquardt method [16]. The update is limited to once to maintain real-time implementation.

The cost function for MHE is formulated bellow. Although the time window changes every time step, the suffix starts from one without losing any generality.

$$\begin{aligned} X = \arg\min_X \Bigg\{ & \frac{1}{2}||x_1 - \hat{x}_1||^2_{P_n} + \frac{1}{2}\sum_{i=1}^{n_h - 1} ||x_{i+1} - f(x_i, u_i)||^2_{Q_n} \\ & + \frac{1}{2}\sum_{i=1}^{n_h} ||y_i - h(x_i, u_i)||^2_{R_n} \Bigg\} \end{aligned} \tag{17}$$

where $||A||_B^2 = A^T B^{-1} A$、 P_n is the covariance of the state x_1. The first term of equation (17) is called the "arrival cost" which is the constraint of the first state vector. The second term is the constraint by state propagation function and the last term is the constraint by the observation function.

MHE is defined by the n_h order Markov process so the arrival cost significantly affects the overall performance of MHE. Particle filter and UKF was applied to estimate $\hat{x}_1$ and P_n [17]. However, the arrival cost is not the focus of this work; thus, x_2 of the previous state is used as $\hat{x}_1$.

All components of equation (17) are square errors; therefore, it can be expressed by the residual vector $R(X)$.

$$X = \arg\min_X R(X)^2 \tag{18}$$

where $R(X)^2 = R(X)^T R(X)$. $R(X)$ are defined as follows.

$$R(X) = \begin{bmatrix} \frac{1}{\sqrt{2}} P_n^{-1/2}(x_1 - \hat{x}_1) \\ \frac{1}{\sqrt{2}} Q_n^{-1/2}(x_2 - f(x_1, u_1)) \\ \vdots \\ \frac{1}{\sqrt{2}} Q_n^{-1/2}(x_{n_h} - f(x_{n_h-1}, u_{n_h-1})) \\ \frac{1}{\sqrt{2}} R_n^{-1/2}(y_1 - h(x_1, u_1)) \\ \vdots \\ \frac{1}{\sqrt{2}} R_n^{-1/2}(y_{n_h} - h(x_{n_h}, u_{n_h})) \end{bmatrix} \tag{19}$$

The optimization problem here is to minimize the square of the residual vector $R(X)$. Therefore, the Gauss-Newton method can be applied. The Jacobian matrix of $R(X)$ is defined as $\frac{dR(X)}{dX} = J(X)$. The state update vector ΔX is the solution of the below equation.

$$J(X)^T J(X) \Delta X = -J(X)^T X \tag{20}$$

Consequently, the state update from time step k to $k+1$ is given by calculating $X^{k+1} = X^k + \Delta X^k$.

C. Gaussian Process based Moving Horizon Estimation

In GP-MHE, the delay time t_d is added to the state vector X. The size of t_d corresponds with the number of external sensors in the vehicle system. To estimate the delayed times, the cost function of MHE should be differentiable by the delay times. The observation data y_i in the third term of equation (17) is discrete; hence, it cannot be differentiated. Therefore, the GP is introduced to convert the discrete data into time differentiable function and applied to equation (17).

The cost function of GP-MHE is formulated as follows.

$$\begin{aligned} X = \arg\min_X \Bigg\{ & \frac{1}{2}||x_1 - \hat{x}_1||_{P_n}^2 + \frac{1}{2}\sum_{i=1}^{n_h-1} ||x_{i+1} - f(x_i, u_i)||_{Q_n}^2 \\ & + \frac{1}{2}\sum_{i=1}^{n_h} ||\hat{y}(t_i' + t_d) - h(x_i, u_i)||_{\hat{R}_n(t_i'+t_d)}^2 \\ & + \frac{1}{2}||t_d - t_d^-||_{S_n}^2 \Bigg\} \end{aligned} \tag{21}$$

where t_d^- is the previously estimated time delay and S_n is the covariance matrix of the delay time propagation and the

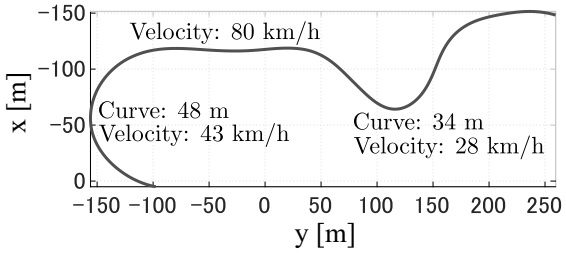

Fig. 6. Vehicle trajectory of full-vehicle simulation.

GP of the discrete data can be expressed by the following function using equation (14) and equation (15).

$$\hat{y}(t') = f_{av}(t') \tag{22}$$

$$\hat{R}_n(t') = f_{var}(t') + R_n \tag{23}$$

In comparison to the conventional MHE, the observation data in the third term of equation (21) became a time differentiable function and an extra term was added to restrict changes in the estimated time delay over time. Subsequently, the residual vector $R(X)$ is modified.

$$R(X) = \begin{bmatrix} \frac{1}{\sqrt{2}} P_n^{-1/2}(x_1 - \hat{x}_1) \\ \frac{1}{\sqrt{2}} Q_n^{-1/2}(x_2 - f(x_1, u_1)) \\ \vdots \\ \frac{1}{\sqrt{2}} Q_n^{-1/2}(x_{n_h} - f(x_{n_h-1}, u_{n_h-1})) \\ \frac{1}{\sqrt{2}} \hat{R}_n(t_1' + t_d)^{-1/2}(\hat{y}(t_1' + t_d) - h(x_1, u_1)) \\ \vdots \\ \frac{1}{\sqrt{2}} \hat{R}_n(t_{n_h}' + t_d)^{-1/2}(\hat{y}(t_{n_h}' + t_d) - h(x_{n_h}, u_{n_h})) \\ \frac{1}{\sqrt{2}} S_n^{-1/2}(t_d - t_d^-) \end{bmatrix} \tag{24}$$

Identical to conventional MHE, the state update vector is calculated by equation (20) to update X.

By adding the delay term at the end of state vector X, the term $J(X)^T J(X)$ becomes a sparse arrow matrix pointing towards lower right direction. This avoids the "fill-in" when LU factorization is carried out and drastically reduces computational load to solve the equation (20) [18]. Therefore, computational time increases linearly with the horizon time. Sparse calculation neglects the zero entries to increase calculation speed thus it is the key to real-time implementation.

IV. Simulation and Experimental Validation

The simulation study was conducted using a full-vehicle simulator, then real vehicle experiment was carried out on a highway scenario. The performance of the two algorithms were evaluated; the proposed GP-MHE and the conventional unscented Kalman filter (UKF) which has no data delay compensation. The horizon time t_w and the sampling rate of the GP-MHE was set to 2s and 50Hz respectively. Average step time of UKF and GP-MHE was 2ms and 10ms respectively with Matlab script using PC with core i7-6700T,

TABLE I

SENSOR ERROR AND TIME DELAY APPLIED FOR SIMULATION

Sensor	Data error
Gyro	Bias: 0.01 deg/s Noise Standard Deviation: 0.005 deg/s
Accelerometer	Bias: 1 mG Noise Standard Deviation: 10 mG
LiDAR localization	Noise: 0.05 m Delay: 100ms
GNSS Doppler Velocity	Noise Standard Deviation: 0.02 m/s Delay: 150 ms

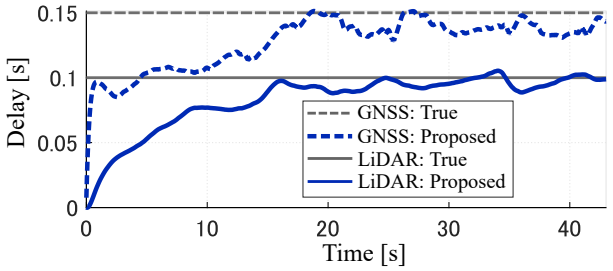

Fig. 7. Estimated delay time by GP-MHE in the simulation study.

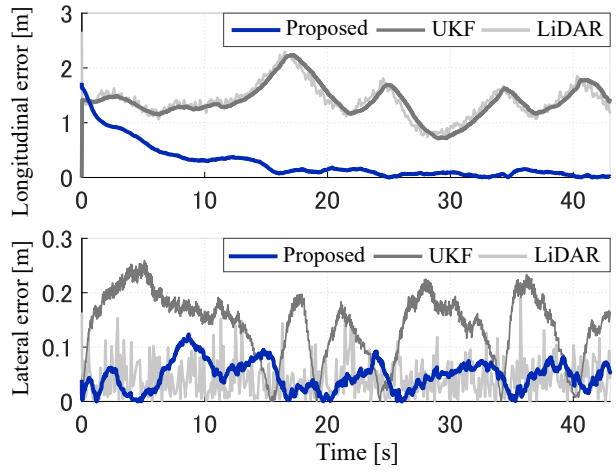

Fig. 8. Localization error with GP-MHE and UKF in simulation study.

A. Full-Vehicle Simulation

The full-vehicle simulator "CarSim" was used to simulate the vehicle dynamics. The simulation trajectory is shown in Fig. 6. The maximum acceleration was set to 0.3G. The IMU, odometry, and steer angle were acquired at 50Hz; the LiDAR and GNSS data were acquired at 10Hz. The errors and time delay added to the sensor data are shown in Tab. I. Different delay times were added to LiDAR and GNSS. All errors were dealt as unknown values.

The estimation results of delay times by GP-MHE are shown in Fig. 7. The estimation errors of LiDAR and GNSS were less than 20ms each after converging. Furthermore, sub 20ms (sampling rate of GP-MHE) resolution of estimated delays were achieved. It is important to note that GP-MHE can estimate individual time delay of multiple sensors.

Localization error by GP-MHE and UKF are shown in Fig. 8. LiDAR data demonstrated large longitudinal errors due to the delay. Similarly, UKF without delay compensation had large longitudinal errors with an unstable lateral error. The proposed GP-MHE achieved sub 0.1m position accuracy as the estimated delays converged to true value. GP-MHE can overcome multiple sensor delays of more than 100ms.

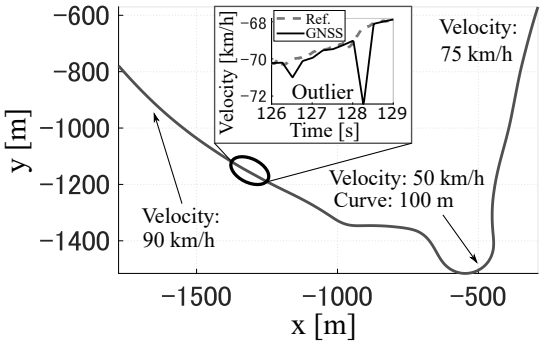

Fig. 9. Vehicle trajectory in the experiment on highway scenario.

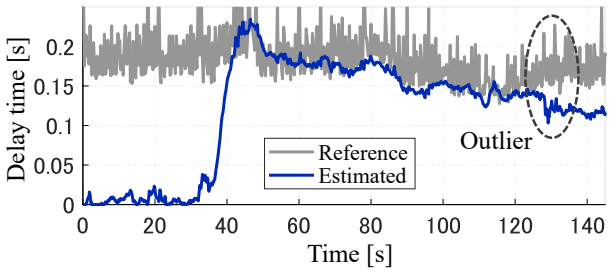

Fig. 10. Estimated delay time by GP-MHE on a highway scenario.

B. Experiment on highway scenario

Fig. 9 shows the highway route used for the experiment that consists of straight roads and interchanges. EPSON IMU M-550 for accelerometer and gyroscope and CAN for steer angle and odometry were acquired at 50Hz. U-Blox GNSS for velocity and position were acquired at 4Hz. An instance of GNSS outlier data was observed at 128s. Applanix POSLV post processed data were used as reference data.

The delay time of the GNSS data were measured accurately by synchronizing onboard PC time to GNSS. The time between GNSS raw data time stamp and the time when the system received the data was regarded as the delay time. The measured reference delay time is shown in Fig. 10, which consisted of slow change and noise. The precondition here was to assume the delay time as unknown value.

The result of delay time estimation by GP-MHE is shown in Fig. 10. The estimated time converged to the reference time when a vehicle approached the interchange. This is because the vehicle should be in dynamic motion for the estimation to progress.

Fig. 11 shows the localization error. The performance of UKF was close to that of the GNSS data. As for the proposed GP-MHE, lateral position error remained stable and longitudinal error converged to less than 0.3 m; thereby achieving sub-meter accuracy. The decrease of longitudinal

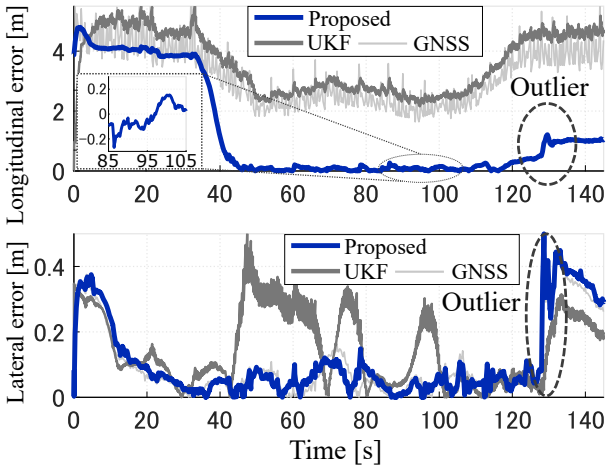

Fig. 11. Localization error with GP-MHE and UKF on a highway scenario.

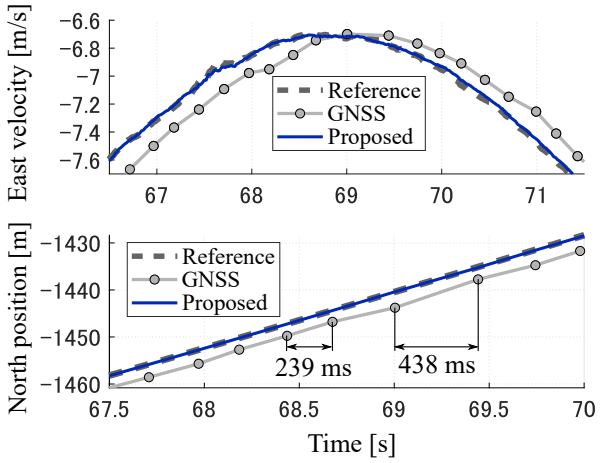

Fig. 12. Estimated velocity and position by GP-MHE on a highway scenario using GNSS data with unknown delay and irregular sampling rate.

error from about 4m to 0.3m is a promising result.

The estimation results of GP-MHE jumped at the point where the GNSS outlier was observed. To further enhance the robustness of the algorithm, outlier detection and exclusion should be considered. Integrating authors previous work on outlier detection and exclusion scheme to GP-MHE is the next challenge [19].

Fig. 12 indicates that the velocity and the position estimation result closely follow the true value; however, the delay time of the GNSS data is unknown. Furthermore, although irregular sampling rate were frequently observed with the GNSS data, GP-MHE showed robust estimation results.

V. Conclusion

In this study, simultaneous estimation of vehicle position and sensor delays using Gaussian process based MHE (GP-MHE) was presented. The GP was applied to convert discrete data into time differentiable functions to estimate unknown delays and position simultaneously in MHE. In the simulation study, the GP-MHE was capable of estimating the delays of two sensors with and accuracy of 20ms each, and the localization error converged to less than 0.1m. Additionally, in the real car experiment on a highway scenario, the proposed method achieved the localization accuracy of 0.3m under unstable data delay of more than 150ms with irregular sampling rate ranging from 250ms to 450ms. The GP-MHE calculation time for each step was in average 10ms and was capable of 50Hz real-time implementation. This algorithm, with its simplicity, has a potential to improve the localization accuracy for not only autonomous systems, but for platooning and other multi-agent control systems. As for the future work, we will further work on enhancing the robustness of the GP-MHE by considering non-Gaussian sensor data and integrating the scheme of authors previous work [19] on fault detection and exclusion.

References

[1] C. Urmson, J. Anhalt et al., Autonomous driving in urban environments: boss and the urban Challenge, Int. J. Field Robot., vol. 25, no. 8, pp.425-466, 2007.

[2] K. Bogdanski and M. C. Best, Kalman and particle filtering methods for full vehicle and tyre identification, Vehicle Syst. Dyn., vol. 56, no. 5, pp.769-790, 2017.

[3] S. Antonov, A. Fehn, and A. Kugi, Unscented Kalman filter for vehicle state estimation, Int. J. Vehicle Mech. Mobility, vol. 49, no. 9, pp.1497-1520, 2011.

[4] T. A. Wenzel, Dual extended Kalman filter for vehicle state and parameter estimation, Vehicle Syst. Dyn., vol. 44, no. 2, pp.153-171, 2006.

[5] A. Gopalakrishnan, N. S. Kaisare, and S. Narasimhan, Incorporating delays and infrequent measurements in extended Kalman filter based nonlinear state estimation, J. Process Contr., vol. 21, pp.119-129, 2011.

[6] Y. Wang, B. M. Nguyen, H. Fujimoto, and Y. Hori, Multirate estimation and control of body slip angle for electric vehicles based on onboard vision system, IEEE T. Ind. Electron., vol. 61, no.2, pp. 1133-1143, 2014.

[7] M, Li and A. I. Mourikis, 3-D motion estimation and online temporal calibration for camera-IMU systems, IEEE Int. Conf. Robot. Autom. pp.5709-5716, 2013.

[8] J. B. Rawlings and B. R. Bakshi, Particle filtering and moving horizon estimation, Comput. Chem. Eng., vol. 30, no. 10-12, pp.1529-1541, 2006.

[9] C. V. Rao, J. B. Rawlings, and D. Q. Mayne, Constrained state estimation for nonlinear discrete-time systems: stability and moving horizon approximations, IEEE T. Automat. Contr., vol. 48, no. 2, pp. 246-258, 2003.

[10] S. Krämer and R. Gesthuisen, Multirate state estimation using moving horizon estimation, IFAC Proceedings, vol. 38, no. 1, pp. 1-6, 2015.

[11] P. Kühl, M. Diehl, T. Kraus, J. P. Schlöder, and H. G. Bock, A real-time algorithm for moving horizon state and parameter estimation, Comput. Chem. Eng., vol. 35, no. 1, pp. 71-83, 2011.

[12] J. Vandersteen, M. Diehl, C. Aerts, and J. Swevers, Spacecraft attitude estimation and Sensor calibration using moving horizon estimation, J. Guid. Control Dynam., vol. 36, no. 3, pp. 734-742, 2013.

[13] M. Zanon, J. V. Frasch, and M. Diehl, Nonlinear moving horizon estimation for combined state and friction coefficient estimation in autonomous driving, European Control Conference (ECC), pp. 4130-4135, 2013.

[14] C. E. Rasmussen and C. K. I Williams, Gaussian Processes for Machine Learning. MIT Press, 2006.

[15] R. Rajamani, Vehicle Dynamics and Control. Springer, 2012.

[16] S. Boyd and L. Vandenberghe, Introduction to Applied Linear Algebra – Vectors, Matrices, and Least Squares. Cambridge University Press, 2018.

[17] S. Ungarala, Computing arrival cost parameters in moving horizon estimation using sampling based filters, J. Process Contr., vol. 19, no. 9, pp. 1576-1588, 2009.

[18] Y. Saad, Iterative methods for sparse linear systems, SIAM, 2003.

[19] D. Mori, H. Sugiura and Y. Hattori, Adaptive Sensor Fault Detection and Isolation using Unscented Kalman Filter for Vehicle Positioning, IEEE Intelligent Transportation Systems Conference (ITSC), New Zealand, pp. 1298-1304, 2019.